Chlorine Solubility in Silicate Melts: New Experiments and Thermodynamic Mixing Model

Journal Article

Author(s):
Aranovich, Leonid Y.; Golunova, Maria A.; Connolly, James A.D.; Ivanov, Mikhail V.

Chlorine Solubility in Silicate Melts:
New Experiments and Thermodynamic Mixing Model

L. Y. Aranovich[a, b], *, M. A. Golunova[a, b], J. A. D. Connolly[c], and M. V. Ivanov[d]

[a] *Institute of Geology of Ore Deposits, Petrography, Mineralogy and Geochemistry,*
Russian Academy of Sciences, Moscow, Russia

[b] *Institute of Experimental Mineralogy, Russian Academy of Sciences, Chernogolovka, Moscow oblast, Russia*

[c] *Institute of Geochemistry and Petrology, Swiss Federal Institute of Technology, Zurich, CH-8092 Switzerland*

[d] *Institute of Precambrian Geology and Geochronology, Russian Academy of Sciences, St. Petersburg, Russia*

*e-mail: lyaranov@igem.ru

Abstract—We present new experimental data on Cl solubility in model basalt melts of eutectic compositions diopside (*Di*)−albite (*Ab*) and *Di*−anorthite ± quartz (*Qtz*). The starting glasses were equilibrated with aqueous NaCl−CaCl$_2$ fluid at 4 kbar in the temperature range of 900−1200°C. The experiments show that Cl solubility decreases with increasing NaCl in the fluid. Ca−Na partitioning between melts and fluid is weekly temperature dependent and resembles that of the plagioclase−fluid system. The newly obtained experimental data, along with previously published results on the model granite melting in the presence of (Na,K)Cl brines (Aranovich et al., 2013), are used to calibrate an empirical thermodynamic model for salt species (NaCl, KCl, and CaCl$_2$) in silicate melt. Calculations show that Cl solubility in haplogranite melt decreases with increasing K/Na ratio in the fluid (and correspondingly, melt). The data acquired on Ca and Na partitioning between melt and fluid make it possible to model the evolution of the Ca/Na ratio in the crystallization course of basalt melts. At a high pressure (10 kbar), Cl solubility in model granite increases with increasing H$_2$O content. The calculated phase diagram for a simple pseudo-ternary system *Ab*−H$_2$O−NaCl demonstrates complex phase relations and, correspondingly, evolution of the H$_2$O and NaCl concentrations in the melt. This complex evolution is illustrated by data on the composition of quartz-hosted melt and fluid inclusions from granites in the Verkhneurmisskii massif in the Badzhal volcano-plutonic zone.

Keywords: silicate melt, chlorine solubility, aqueous chloride fluid, experiments, thermodynamics, fluid-magmatic evolution

INTRODUCTION

Chlorine, along with H$_2$O, CO$_2$, S, and F, is one of the most important volatile components dissolved in magmas. In magma−fluid systems, effects of Cl on phase equilibria (Filiberto and Treiman, 2009; Aranovich, 2017), the evolution of magmatic fluids (Lukanin, 2015, 2016), and metasomatic transformations (Aranovich and Safonov, 2018; Kusebauch et al., 2015; Safonov and Aranovich, 2014) are disproportionally important, given the relatively low planetary abundance of this element (Patiño Douce et al., 2011). Chloride ligands control the solubility of most ore metals in fluids of magmatic mineral deposits (Rubtsova et al., 2023 and references therein). The occurrence of Cl and its soluble salts also controls the pH of magmatic fluids (Holland, 1972; Ryabchikov, 1975). Variations in this parameter due to magmatic differentiation processes at the cooling and/or ascent of melts, as well as those induced by interaction between magmatic fluid, host rocks, and meteoric solutions, principally affect metasomatic and transport processes and the deposition of ore metals.

Chlorine solubility in silicate melts has been studied by many experimentalists (Webster et al., 2015; Dolejš and Zajacz, 2018; Chevychelov, 2019; Hsu et al., 2019; Thomas and Wood, 2023; and references therein). A large set of experimental data on systems of complex composition was used to derive empirical equations for describing Cl solubility as a function of temperature, pressure, and composition of felsic (Lukanin, 2015; Dolejš and Zajacz, 2018) and mafic (Webster et al., 2015; Thomas and Wood, 2023) melts. Witham et al. (2012) have proposed a model for Cl partitioning between mafic melts and C−O−H−S−Cl fluid. The partitioning of cations between melts and Cl-bearing fluids is much less studied, despite this problem is extremely important for modeling the compositional evolution of fluid segregated during magma degassing. No models have been proposed so far that would describe Cl solubility in melts and could be uti-

lized in currently widely used petrological program packages for calculating phase equilibria in natural systems. This significantly hampers (or even makes impossible) reasonably accurate simulations of the evolution of magma−fluid systems.

This publication presents our newly acquired experimental data on Cl solubility in haplobasalt melts depending on their composition and chloride concentrations with known activities of the salts in the fluid phase. The paper also reports estimated Ca and Na partitioning between melt and aqueous saline fluid. Considered together with previous experimental data on the melting of model granite in the presence of aqueous (K,Na)Cl solution (Aranovich et al., 2013), these data were employed to develop a thermodynamic model for silicate melts containing K, Ca, and Na chlorides and to evaluate Ca and Na partitioning between basalt melt and fluid and K and Na partitioning between granite melt and fluid, which is principally important to reproduce the compositional evolution of fluid segregating from magma at its crystallization and to understand the nature of metasomatic processes occurring when host rocks interact with magmatic fluids.

EXPERIMENTAL EQUIPMENT AND METHODS

Experimental Equipment

The experimental runs were carried out using IHPV, with Ar as the pressure medium. The pressure was measured by a spring-tube manometer accurate to ±20 MPa. All runs were carried out at 400 MPa. The temperature was measured by two Pt−PtRh10 thermocouples, whose hot junctions were positioned at the top and bottom ends of the copper holder into which four to six platinum capsules (50 × 5 × 0.2 mm) with starting materials were placed. Temperature was measured and controlled in the course of the runs with a MINITHERM temperature responsive controller and was determined accurate to ±5°C. The runs were conducted within the temperature range of 900−1200°C. The run duration was 5 days, which is sufficient to reach equilibrium in the system (Shaposhnikov and Aranovich, 2015).

Starting Materials

The starting materials were glasses compositionally approximating the eutectics diopside (*Di*)−anorthite (*An*) ($Di_{58}An_{42}$, wt %) with varied quartz contents (0−20 wt % *Qtz*), *Di*−albite (*Ab*) ($Di_{11}Ab_{89}$, wt %), and $Di_{11}Ab_{89}$ + 2 wt % NaCl. The glasses of corresponding composition were prepared in open Pt capsules at 1450°C in a high-temperature tube furnace (Borisov and Aranovich, 2019) for 24 h from mixtures of Na_2CO_3, Al_2O_3, SiO_2, $CaCO_3$, $Mg(OH)_2$, and NaCl (all chemically pure), which were carefully mixed in

desired proportion in an agate mortar under acetone. The glasses thus made (25−30 mg) and desired amounts of deionized H_2O and salt (NaCl or $CaCl_2$, which had been carefully dried before loading) were loaded into Pt capsules using the weight technique. All weighings were done using a Mettler-Toledo analytic balance, which guarantees a reproducibility to ±0.02 mg. Upon their loading, the capsules were arc-welded in Ar and weighed to check possible weight losses on welding. The experimental parameters and weight proportions of the starting materials are summarized in Table 1. Four to six capsules were simultaneously run in the IHPV. The runs were quenched by rapidly dropping the capsules into cold water. After the runs, the capsules were dried and weighed to check for possible weight losses.

Analysis of Experimental Products

The content of the capsules after runs (silicate glasses and solutions) was carefully collected into Petri dishes. The solutions were collected by decanting into measuring tubes and then diluted to an aliquot of 5 ± 0.1 mL with a required amount of deionized H_2O. The solutions were analyzed for Na and K cations by flame photometry on a FPA-2-01 flame photometer in gas−air flame. Ca was analyzed by atomic absorption spectrometry on a Shimadzu 7000 spectrometer in acetylene−air flame. The glasses (quenched melts) were dried in a muffle furnace at 110°C and used to make pellets with epoxy resin. The pellets were carefully polished and then analyzed by EPMA on a JEOL Superprobe 8200 with five spectrometers at the Institute of Geology of Ore Deposits, Petrography, Mineralogy and Geochemistry, Russian Academy of Sciences. The analysis was carried out at an accelerating voltage of 15−20 kV, sample current of 10 nA, with the beam focused to a spot 5−10 μm in diameter. Natural diopside and sanidine were the standards in analysis for Si, Al, Ca, and K; $Na_2BeSi_2O_6$ was the standard for Na (with a correction introduced for the possible Na losses; see Andreeva et al., 2018); and synthetic atacamite $Cu_2Cl(OH)_3$ was used for Cl.

EXPERIMENTAL RESULTS

In most of the runs, silicate melts were quenched into homogeneous glasses that contained variable amounts of fluid inclusions, which had been entrapped in the course of the runs and on quenching (Fig. 1a). The products of some of the runs at 900 and 1000°C contained minor amounts (no more than 10%) of quenched clinopyroxene crystals of composition close to diopside (Fig. 1b). The products of the experimental runs of Set 4, with $Di_{58}An_{42} \pm Qtz$ starting glass (Table 1), contained up to 80−90 vol % quenched clinopyroxene grains of the total volume of the run product (visual evaluations in BSE images, Fig. 1c). The quenched nature of the clinopyroxene is

Table 1. Parameters of experimental runs on Cl solubility in haplobasalt melts at 4 kbar

Run	T, °C	Starting glass	Glass	$CaCl_2$	NaCl	H_2O
1–3	1000	$Di_{11}Ab_{89}$	29.9	3		13.5
1–4	1000	$Di_{11}Ab_{89}$ + NaCl	30	3		13.7
1–7	1000	$Di_{11}Ab_{89}$	29.9		2	17.2
1–8	1000	$Di_{11}Ab_{89}$ + NaCl	30		2	17.2
2–1	1000	$Di_{11}Ab_{89}$	24.8		4.9	17.1
2–2	1000	$Di_{11}Ab_{89}$	25		8	17.2
2–3	1000	$Di_{11}Ab_{89}$	25.3		12.1	17.1
2–4	1000	$Di_{11}Ab_{89}$ + NaCl	25.2		4.9	17
2–5	1000	$Di_{11}Ab_{89}$ + NaCl	25.4		8.2	17
2–6	1000	$Di_{11}Ab_{89}$ + NaCl	24.8		12	17
2–7	1000	$Di_{11}Ab_{89}$	25.1	7.2		14.2
2–8	1000	$Di_{11}Ab_{89}$	25	10		14.1
2–9	1000	$Di_{11}Ab_{89}$	25.1	15.1		14
2–10	1000	$Di_{11}Ab_{89}$ + NaCl	25.2	7		14.1
2–11	1000	$Di_{11}Ab_{89}$ + NaCl	25	10.1		14.2
2–12	1000	$Di_{11}Ab_{89}$ + NaCl	24.8	15		14
2–13	1000	$Di_{58}An_{42}$ + 10% Qtz	25		5.2	17.1
2–14	1000	$Di_{58}An_{42}$ + 10% Qtz	25.1		8	17.2
2–15	1000	$Di_{58}An_{42}$ + 10% Qtz	25		12.1	17
2–16	1000	$Di_{58}An_{42}$ + 20% Qtz	25.4		5.1	17.2
2–17	1000	$Di_{58}An_{42}$ + 20% Qtz	25.6		8.2	17.1
2–18	1000	$Di_{58}An_{42}$ + 20% Qtz	25		12.1	17
3–1	1100	$Di_{11}Ab_{89}$	20.3		5.1	17.2
3–2	1100	$Di_{11}Ab_{89}$	20		8	17.1
3–3	1100	$Di_{11}Ab_{89}$	20.2		12.2	17.2
3–4	1100	$Di_{11}Ab_{89}$ + NaCl	23.3		5	17
3–5	1100	$Di_{11}Ab_{89}$ + NaCl	22.9		7.9	17
3–6	1100	$Di_{11}Ab_{89}$ + NaCl	23.4		12	17.1
4–1	1200	$Di_{58}An_{42}$	25.4	3.1		13.7
4–2	1200	$Di_{11}Ab_{89}$	25	3.1		13.5
4–3	1200	$Di58An_{42}$	25.3		2	17.2
4–4	1200	$Di_{11}Ab_{89}$	25		2.2	17.3
4–5	1200	$Di_{58}An_{42}$	25.3	9.2		13.6
4–6	1200	$Di_{11}Ab_{89}$	25	9		13.6
4–7	1200	$Di_{58}An_{42}$	25.4		6.1	17.4
4–8	1200	$Di_{11}Ab_{89}$	25.4		6	17.2
5–1	900	$Di_{11}Ab_{89}$	26.7		5.1	20.2
5–2	900	$Di_{11}Ab_{89}$	25.6		8.1	20
5–3	900	$Di_{11}Ab_{89}$	25.9		12.1	20

All runs lasted 5 days. All weights in Table 1 are in mg.

(a)   100 μm

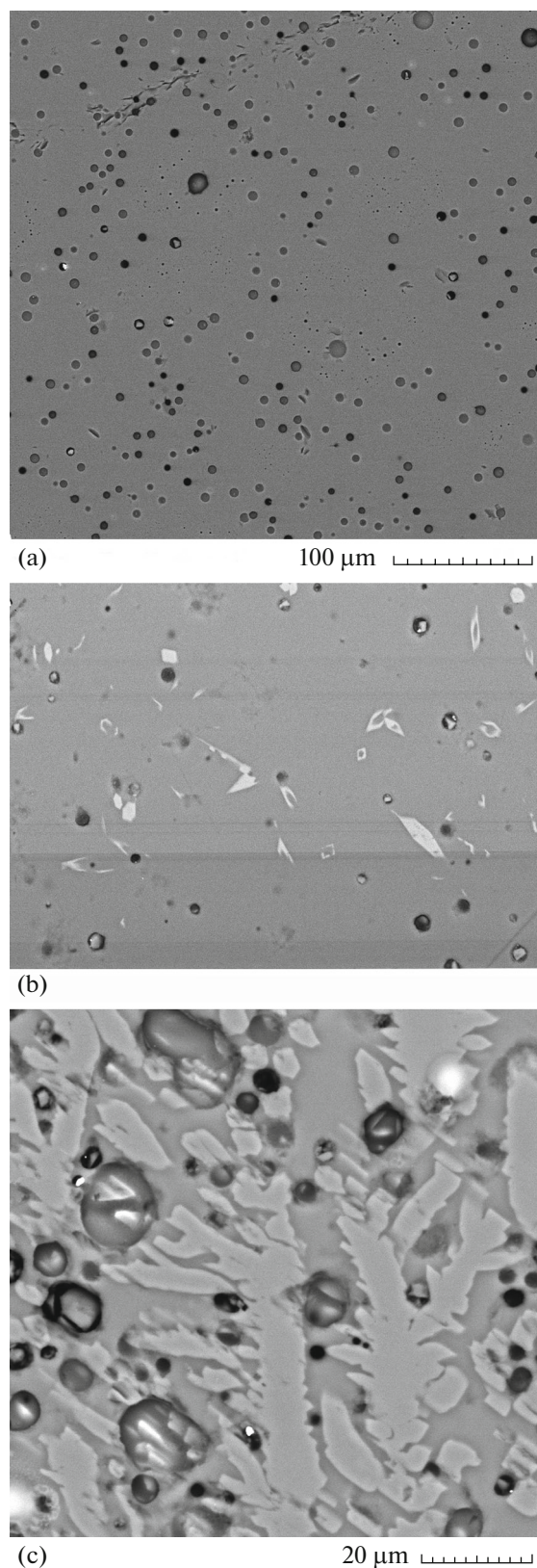(b)

(c)   20 μm

Fig. 1. BSE images of glasses in the products of runs (a) 2-8, (b) 5-3, and (c) 4-5. Brighter grains in Figs. 1a and 1b are quenched clinopyroxene of composition close to diopside. Images in Figs. 1b and 1c were taken at the same magnification.

evident from the morphology of the feather-shaped (Fig. 1b) and dendritic (Fig. 1c) grains and from the specific composition with unequilibrated Ca/Mg > 1.

The composition of the glasses (EPMA data) and equilibrium solutions are reported in Table 2. For the runs whose products contained quench clinopyroxene, the real composition of the melt was recalculated with regard to the amount of the quench grains. Of course, this introduced an additional inaccuracy into the determination results, particularly in the runs with high contents of quench phases (Fig. 1c, these runs are marked with asterisks in Table 2).

DISCUSSION

The Ca and Na partition between the melt and fluid is displayed in Fig. 2. The partition is obviously nonideal and weakly depends on temperature. The partition isotherm of 1200°C, which is drawn provisionally, reasonably well describes the experimental results and is very close to the curve showing exchange between fluid and plagioclase at 700°C according to (Shmulovich and Graham, 2008), which indicates that the mixing properties of the components $CaAl_2Si_2O_8$ and $NaAlSi_3O_8$ in haplobasalt melt and the anorthite and albite end members in the plagioclase solid solution are similar. The significant scatter of the experimental results at different temperatures (likely due to analytical uncertainties of the phases and, particularly, the occurrence of quench crystals) did not allow us to identify any clear temperature dependence of the partitioning.

An important result obtained in this study is the identification of a dependence of Cl concentration in haplobasalt melt on the Ca/(Ca + Na) ratio of this melt (Fig. 3a) and coexisting fluid (Fig. 3b): Cl solubility increases nonlinearly from 0.2–0.3 wt % in the Ca-poor melts to >2 wt % in the Na-poor ones. This result is in agreement with experimental data obtained at a lower pressure (Chevychelov, 2019; Chevychelov and Suk , 2003) and with the empirical equation for the dependence of melt chlorine capacity on its composition (Thomas and Wood, 2023). This result indicates that at the deep-sitting crystallization of basalt magma with a constant initial Cl concentration, the first fluid portions segregating from the magma should be enriched in Na, i.e., bring about the "early" sodic profile of the metasomatic processes at interaction with host rocks.

Chlorine concentration in the melts negatively correlates with the Mg/(Mg + Ca) ratio (Fig. 3c). This correlation, although not clearly discernible in our runs, indicates that the early crystallization of relatively Mg-rich phases should lead to gradual Cl enrichment in the residual melt.

Table 2. Glass composition (elements in wt %) and Ca mole fraction in glass (m) and fluid (fl) in the products of experiments on Cl solubility in haplobasalt melts at 4 kbar

Run	T, °C	Na	Mg	Al	Si	Cl	Ca	O	Ca/(Ca + Na), m	Ca/(Ca + Na), fl
1-3	1000	2.84	1.16	9.14	29.66	0.27	5.07	45.70	0.412	0.098
1-4	1000	2.59	0.52	8.79	30.34	0.43	4.88	45.58	0.519	0.088
1-7	1000	4.50	1.26	9.08	29.72	0.30	2.89	45.49	0.122	0.055
1-8	1000	4.28	1.25	8.15	30.79	0.15	2.76	45.74	0.110	0.038
2-1	1000	5.85	1.01	11.38	27.33	0.58	2.37	44.95	0.189	0.025
2-2	1000	7.26	0.91	9.37	28.73	0.89	1.62	44.72	0.114	0.011
2-3	1000	7.37	0.95	9.86	29.24	0.67	1.25	45.69	0.089	0.008
2-4	1000	6.15	0.93	10.40	28.65	0.54	1.90	45.45	0.151	0.011
2-5	1000	6.63	0.98	11.35	27.20	0.67	1.95	44.86	0.144	0.002
2-6	1000	7.38	0.95	8.68	29.26	0.97	1.56	44.88	0.107	0.001
2-7	1000	1.15	0.72	9.45	27.33	1.85	9.05	44.07	0.820	0.457
2-8	1000	0.96	0.69	10.01	26.28	2.06	9.34	43.37	0.848	0.518
2-9	1000	0.65	0.51	9.44	27.61	1.92	8.48	43.82	0.883	0.696
2-10	1000	1.67	0.76	9.14	26.87	1.83	8.80	43.36	0.751	0.270
2-11	1000	0.90	0.52	9.35	27.37	1.69	8.85	43.73	0.850	0.456
2-12	1000	3.58	2.14	9.73	24.21	1.26	9.12	42.54	0.593	0.428
3-1	1100	5.53	0.50	8.76	30.61	0.56	1.88	45.73	0.163	0.004
3-2	1100	6.11	0.97	8.90	29.90	0.69	1.97	45.64	0.155	0.008
3-3	1100	6.37	0.81	8.88	30.25	0.61	1.50	45.79	0.120	0.006
3-4	1100	5.70	1.03	8.62	30.59	0.41	2.11	46.11	0.175	0.007
3-5	1100	5.69	0.77	9.06	29.93	0.57	2.53	45.73	0.205	0.009
3-6	1100	6.12	1.02	8.87	30.34	0.48	1.69	46.01	0.137	0.005
4-1*	1200	0.00	5.97	6.63	21.37	1.35	18.33	41.60	0.983	0.755
4-2	1200	4.47	0.82	7.66	30.22	1.39	4.70	45.28	0.376	0.073
4-3*	1200	1.17	3.35	8.18	22.48	0.57	16.66	42.23	0.899	0.470
4-4	1200	6.35	0.78	8.18	30.76	0.32	1.95	45.90	0.150	0.012
4-5*	1200	0.06	5.33	7.25	21.58	1.08	17.85	41.75	0.993	0.801
4-6	1200	1.57	0.58	7.91	29.03	1.76	9.12	44.69	0.769	0.355
4-7*	1200	2.64	1.55	10.01	23.73	0.74	13.18	43.16	0.742	0.214
4-8	1200	5.60	0.69	8.23	31.43	0.40	1.78	46.27	0.155	0.022
5-1	900	6.07	1.47	7.80	30.54	0.19	2.64	45.87	0.084	0.004
5-2	900	6.51	0.74	8.18	31.28	0.21	1.54	46.28	0.081	0.007
5-3	900	6.60	0.91	8.06	30.99	0.63	1.54	46.00	0.078	0.005

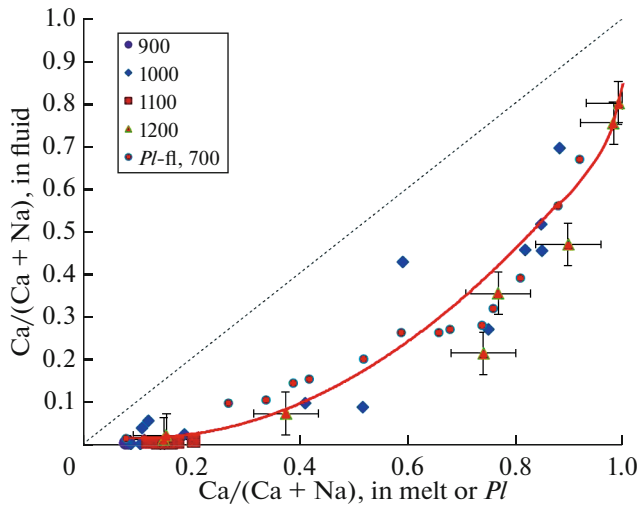* The products of these runs contain much quenched glass.

Fig. 2. Ca and Na partitioning between haplobasalt melt and aqueous chloride fluid: experimental data at 4 kbar.

Legend: temperature is in °C, red line is the isotherm of 1200°C (provisional data); the thin continuous line shows equal Ca/(Ca + Na) values. The error brackets are shown for the runs at 1200°C. Red circles are data of experiments on Ca−Na exchange between fluid and plagioclase (*Pl*) according to (Shmulovich and Graham, 2008).

THERMODYNAMIC MODEL OF Cl-BEARING SILICATE MELTS

Experimental data of this study and those of (Aranovich et al., 2013; see also Supplementary[1] 1, ESM_1 and ESM_2), make it possible to calculate parameters of thermodynamic models for Cl-bearing basalt and granite melts, because the experiments were carried out in the presence of fluid with known mixing properties (Aranovich and Newton, 1996, 1997; Ivanov et al., 2019; Ivanov, 2023), and the equilibrium compositions of both phases (glasses, i.e., the quenched melt, and fluid) have been directly analyzed.

Studies of Cl-bearing silicate melts by the structure-sensitive methods (Dalou and Mysen, 2015; Evans et al., 2008) have shown that Cl in the melt forms clusters with major network-modifying cations. In view of this, we assumed that the standard states of chlorides in both melt and fluid are molten pure salts (NaCl, KCl, and $CaCl_2$). Equilibrium condition of chlorides in melt and fluid are then written as

$$a_i(m) = a_i(fl), \qquad (1)$$

[1] Supplementary materials for the Russian and English on-line versions available at https://elibrary.ru/ and http://link.springer.com/, respectively, present.
Supplementary 1: ESM_1.xlsx—Composition of glass in runs on melting of model granite after (Aranovich et al., 2013); ESM_2.xlsx—Compositions of solutions from runs on melting of model granite and basalts. Supplementary 2: Statistical characteristics of multiple regression.
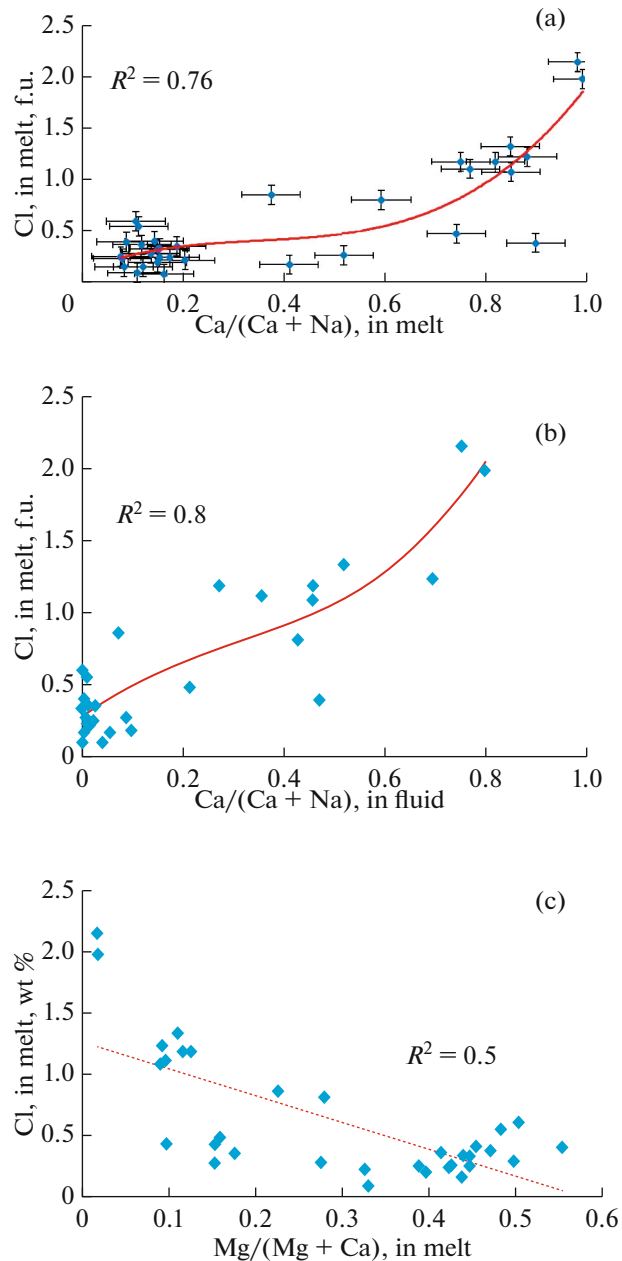

Fig. 3. Dependence of Cl solubility in haplobasalt melt on the Ca/(Ca + Na) ratio of (a) the melt and (b) fluid and (c) Cl solubility in haplobasalt melt depending on the Mg(Mg + Ca) ratio of the melt.

Symbols are experimental data (with error bars in Fig. 3a). Red curves in Figs. 3a and 3b are correlations according to (a) quadratic and (b) cubic equations.

where a_i is the thermodynamic activity of salt i in melt (m) or fluid (fl)

$$a_i = X_i \exp\left[G^{ex}(i)/(RT)\right]. \qquad (2)$$

In Eq. (2), X_i is the mole fraction of chloride, $G^{ex}(i)$ is the excess partial Gibbs free energy of salt i, T is the

temperature in K, and R is the universal gas constant, 8.314 J/(K mol).

The equations for $G^{ex}(i)$ in $H_2O-NaCl-KCl$ and $H_2O-NaCl-CaCl_2$ are presented in (Aranovich and Newton, 1996, 1997) and (Ivanov et al., 2019; Ivanov, 2023), respectively. The activity values of fluid components in the experiments are reported in Supplementary 1, ESM_2.

The total Cl concentrations in the experimental glasses were no higher than 2.15 wt %, i.e., the melts can be confidently regarded as diluted solutions of the chlorides. To describe their mixing properties, we applied empirical equations that were close to Darken's formalism (Darken, 1967; Aranovich, 1991). Because the variations in concentrations of all major components except Na and Ca in basalts and Na, K, and H_2O in granites are very minor, these equations can be written as

$$G_1^{ex} = J_1 + X_1 W_{1(1)} + X_2 W_{2(1)} + X_{H_2O} W_{H_2O(1)} \quad (3a)$$

$$G_2^{ex} = J_2 + X_1 W_{1(2)} + X_2 W_{2(2)} + X_{H_2O} W_{H_2O(2)}. \quad (3b)$$

In Eqs. (3a) and (3b), G_i^{ex} is the partial excess free Gibbs energy of component i, subscript indexes 1 and 2 denote salt components of melts (NaCl and $CaCl_2$ for basalts and NaCl and KCl for granites), X_i is the mole fractions of corresponding melt components, $W_{i(j)}$ is energy parameters (kJ/mol) pertaining to the excess energy of component i that characterize the total interaction of salts 1 and 2 with major components of the melts, and J_i are constants corresponding to the Henry constant. In processing the data on granite, this constant was represented according to the Gibbs−Helmholtz equation as a linear function of temperature (in K) and pressure (in kbar)

$$J_i = A_i + B_i T + C_i P. \quad (4)$$

The experiments on Cl solubility in basalts were conducted at a single pressure $P = 4$ kbar and almost constant H_2O content in the melt (about 5−6 wt % at 900−1200°C and 4 kbar according to the equation in Papale et al., 2006). Because of this, the last summands in Eqs. ((3a), (3b), and (4) were omitted in fitting these data.

We assumed in the calculations that the mole fractions of salts in the melts were proportional to the bulk molar ratios of the respective cations, which leads to the following relations for the calculation of the mole fractions of salts in haplobasalt melt:

$$X_1 = X(NaCl)^m = Na/(Na + Ca)^m \times [Cl]^m, \quad (5a)$$

$$X_2 = X(CaCl_2)^m = Ca/(Na + Ca)^m \times [Cl]^m. \quad (5b)$$

The expression for the mole fractions of salts in model granite melt assumes the form

$$X_1 = X(NaCl)^m = Na/(Na + K)^m \times [Cl]^m, \quad (5c)$$

Table 3. Thermodynamic parameters (kJ/mol) involved in Eq. (3)

Parameter		Basalt	Granite
$W_{na(na)}$		−94.0	75.3
$W_{na(ca)}$		8.6	−
$W_{na(k)}$		−	1215
$W_{ca(na)}$		−364.1	−
$W_{ca(ca)}$		172.2	−
$W_{k(na)}$		−	−516
$W_{k(k)}$		−	1098
$W_{h2o(na)}$		−	−3.56
$W_{h2o(k)}$		−	−15.0
J_1	A	2.37	14.072
	B	10.23	13.851
	C	−	−830.0
J_2	A	−130.7	−13.079
	B	64.7	31.22
	C	−	−963.7

$W_{i(j)}$ are parameters in Eqs. (3a) and (3b) calculated for salt component i in melt in equilibrium with component j in the fluid; na is NaCl, k − KCl, ca is $CaCl_2$, and $h2o$ is H_2O.

$$X_2 = X(KCl)^m = K/(Na + K)^m \times [Cl]^m. \quad (5d)$$

In Eqs. ((5a)−(5d), symbols of elements denote their mole fractions in melts normalized to eight oxygen ions.

Experimental data in Table 2 and Supplementary 1 were used in evaluating parameters involved in Eq. (3) with regard to (4) and (5a)−(5d). The calculations were done by means of linear regression, because Eqs. (3a) and (3b) are linear with respect to the parameters to be refined. The results are presented in Table 3, and Supplementary 2 lists all statistical characteristics of the regression. The parameters of the basalts have large uncertainties and should be considered as tentative (the multiple regression coefficients are 0.82 and 0.68 for NaCl and $CaCl_2$), which is related to the aforementioned uncertainties in the determined compositions of the experimental melts. Also, the equation used to calculate the activities of salts in $H_2O-NaCl-CaCl_2$ fluid (Ivanov, 2023) may probably need to be refined (Makhluf et al., 2023). The parameters calculated for model granite are much more reliable (the multiple regression coefficients are 0.94 and 0.91, respectively, for NaCl and KCl, see Supplementary 2). Selected calculation results on granite obtained with parameters from Table 3 are presented in Figs. 4 and 5.

For haplogranite, Cl solubility in melt seems to show a complex dependence on the melt composition (Figs. 4a, 4b): it slightly increases with increasing H_2O content at a high pressure (Fig. 4a), which is opposite
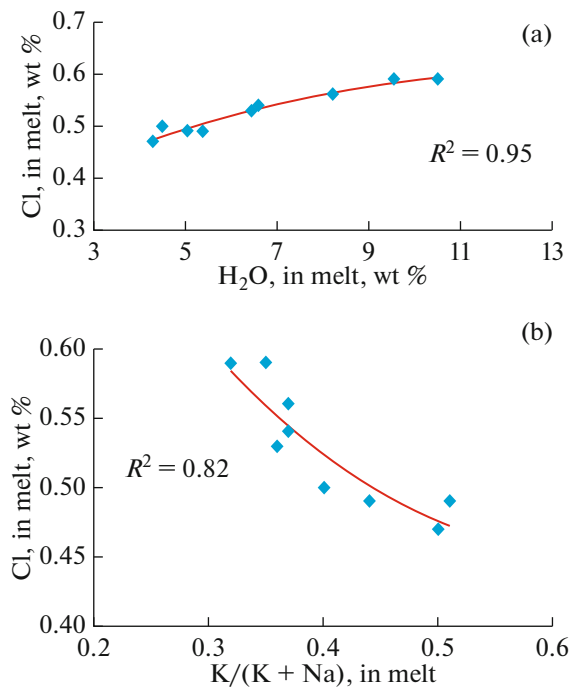
Fig. 4. Cl concentration in model granite melts at 900°C and 10 kbar depending on (a) the H_2O content and (b) $K/(K + Na)$ ratio.

Blue rhombs are experimental points (Aranovich et al., 2013; see Supplementary 1, ESM_1, ESM_2), and red curves are calculations.

to the dependence identified in shallow-depth melts (at 1−3 kbar; e.g., Webster et al., 2015). The most likely reason for this is drastic changes in the activity−composition relations in the saline aqueous fluid (Aranovich and Newton, 1996, 1997). This trend also indicates that salts dissolved in melt partly occur in the form of clusters related to molecular H_2O.

The decrease in Cl solubility with an increase in the $K/(K + Na)$ ratio of the melt (Fig. 4b) is in good agreement with the results obtained in low-pressure (1−3 kbar) experiments (Chevychelov, 2019). An important implication of this result is that, when Cl-bearing granite magmas reach saturation, fluids relatively enriched in K_2O are the first to separate from these magmas, and these fluids can induce potassic metasomatism when interacting with host rocks.

Figure 5 shows an isobaric−isothermal (800°C, 5 kbar) section of the phase diagram of the system albite Ab−H_2O (w)−NaCl (hlt), which was calculated using the Perple_X program complex (Connolly, 2005, 2017, ver. 7.1.0) with the thermodynamic database (Holland and Powell, 2011), mixing parameters for Ab melt−H_2O from (White et al., 2014), and a model for H_2O−NaCl fluid according to (Aranovich and Newton, 1997). According to the model [Eqs. (3a) and (3b)] and parameters from Table 3, the expression for NaCl activity in this system assumes the form (T is temperature in K, and P is pressure in bar)
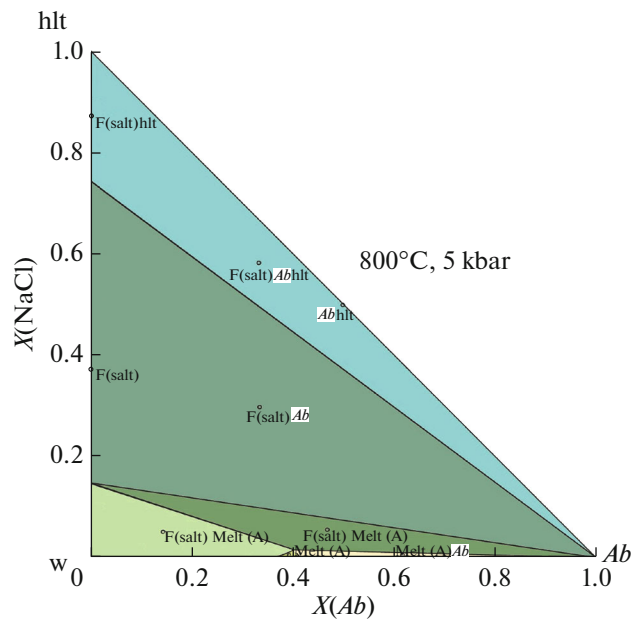

Fig. 5. Isobaric−isothermal (800°C, 5 kbar) section of the phase diagram of the pseudoternary system albite Ab−H_2O (w)−NaCl (hlt). Fields of different color show the stability of various phase associations. Symbols: F(salt) is NaCl-bearing fluid, and Melt is NaCl-bearing melt.

$$RT \ln a (NaCl)^m = 14072 + 13.851T - 0.83P$$
$$+ 75341X (NaCl)^m - 3561X (H_2O)^m \quad (6)$$
$$+ RT \ln X (NaCl)^m.$$

The expressions for the partial excess mixing Gibbs energy for Ab and H_2O were appended with terms pertaining to interaction with NaCl according to a regular solution model.

The diagram in Fig. 5 illustrates the fairly complex relations even in this very simple fluid−mineral system with an aqueous saline solution. It is important to mention the very narrow stability field of albite melt: the maximum NaCl concentration in the fluid at which melting is possible (at given P−T parameters) is $X(NaCl) = 0.15$, $X(H_2O) = 0.85$, and hence, no Cl can be incorporated into melt in the absence of H_2O [$X(H_2O) = 0$] (compare with the diagram in Webster et al., 2015, Fig. 1). NaCl concentration in the melt decreases with increasing H_2O content (Fig. 6a) only in the region where fluid occurs in equilibrium with melt (±albite), which is obviously caused by the decrease in NaCl concentration in the coexisting fluid. Therewith the maximum (and constant) salt concentration in the melt (0.76 wt % NaCl) is reached within the invariant (at constant P and T) field F(salt)−$Melt$−Ab (red rhomb in Fig. 6a).

To elucidate in more detail how H_2O content affects NaCl solubility in melt, we have calculated concentrations of these components in albite melt at
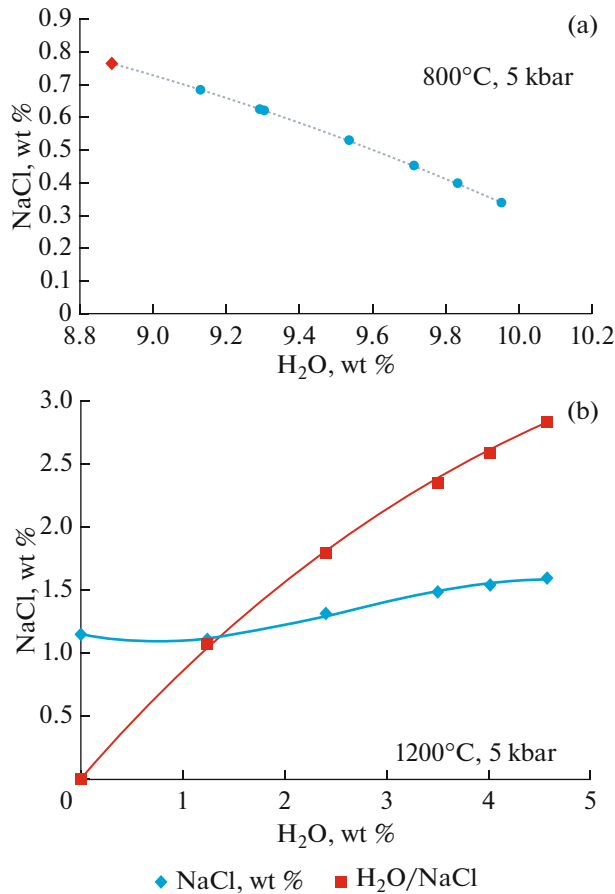
Fig. 6. Relation between water and salt concentrations in fluid-saturated melts in the system $Ab-NaCl-H_2O$ at (a) 5 kbar, 800°C and (b) 1200°C

Symbols are calculated data, curves are interpolations. The rhomb in Fig. 6a is the composition in the invariant albite−melt−fluid field.

Fig. 7. Correlation trends for H_2O and silica concentrations in (a) quartz-hosted melt inclusions in granites from the Verkhneurmiiskii massif (Bortnikov et al., 2019) and (b) model calculations of the isobaric ($P = 5$ kbar) crystallization of granite melt.

The quartz fraction in Fig. 7b is shown relative to the whole quartz amount that crystallized from the melt. Calculation in Fig. 7b pertain to trend A in Fig. 7a.

5 kbar and 1200°C, a temperature at which silicate melt is stable at any salt concentration in the fluid, up to anhydrous NaCl melt (Tenner et al., 2007). Figure 6b shows the calculation results for an arbitrarily selected bulk salt concentration, $X(NaCl) = 0.5$, and variable H_2O content, $X(H_2O) = 0$ to 0.4. As seen in this figure, the dependence of salt concentration in albite melt on the water content at these calculation conditions is principally different from that in Fig. 6a: at a low H_2O content (no higher than 1 wt %), the NaCl concentration is slightly lower than in equilibrium with anhydrous salt melt, and this concentration then slowly increases. Therewith the $H_2O/NaCl$ ratio rapidly increases (and tends to infinity for pure H_2O fluid).

EVOLUTION OF MAGMATIC FLUID SEGREGATING FROM GRANITE

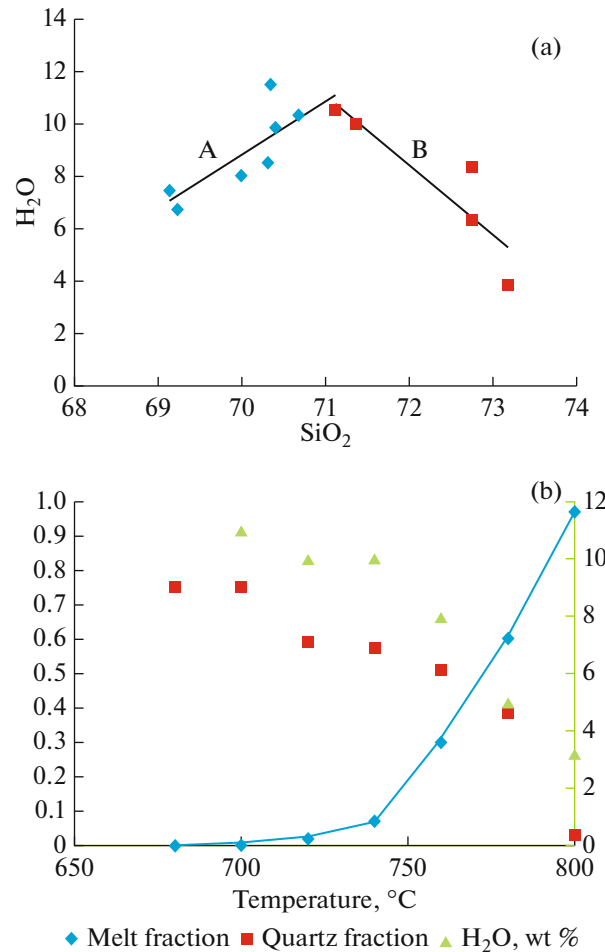Figure 5 shows that the field of fluid-undersaturated melts [without F(salt] is very small and is

bounded by the maximum salt concentration $X(NaCl) = 0.04$ (which corresponds to approximately 0.2 wt % in recalculation to Cl). Even at this fairly low Cl concentration (this value is close to that most commonly found in melt inclusions, e.g., Kovalenko et al., 2000), the first fluid portions segregating from melt are high-concentration brines with $X(NaCl) = 0.15$, which corresponds to approximately 36 wt % NaCl. Although the fraction of brine in the overall budget of segregated fluid is relatively small, its ability to extract many ore metals can be very significant (e.g., Tattitch and Blundy, 2017; Kouzmanov and Pokrovski, 2012). As the melt fraction decreases, the fluid segregated from it should become progressively more diluted (Fig. 6a), up to almost pure H_2O during final crystallization stages.
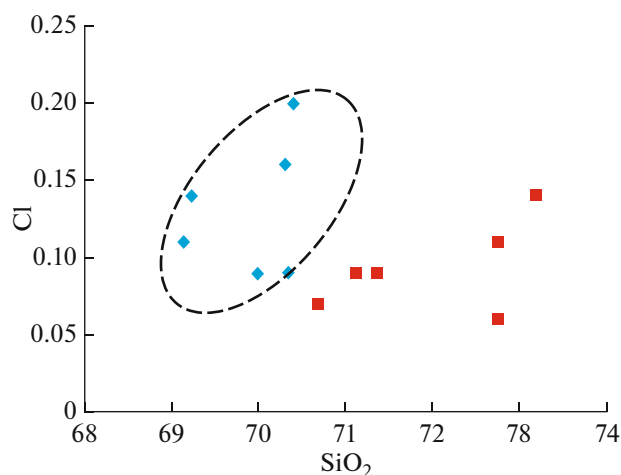
Fig. 8. Correlation trends for Cl and silica concentrations (wt %) in melt inclusions. Lozenges pertain to the composition of the earlier inclusions shown in Fig. 7a and, supposedly, corresponding to the respective evolution in a deep chamber, squares are inclusions captured during decompression.

Extensive empirical data on the composition of melt and fluid inclusions in minerals highlight the complex evolutionary histories of mineral deposits related to granitoid magmatism (see recently published reviews in Blundy et al., 2021; Goldfarb and Pitcairn, 2022). As an example, Fig. 7a shows estimates of H_2O and silica concentrations in melt inclusions hosted in quartz from granites of the Verkhneurmiiskii massif of the Badzhal volcano-plutonic zone, which hosts tin−tungsten deposits (Bortnikov et al., 2019). The diagram shows two clearly distinct trends: one with a positive (A) and the other with a negative (B) correlation between these parameters. Trend A is readily explained by the successive capture of inclusions during the crystallization differentiation in a deep magma chamber (Fig. 7b): the early quartz, which crystallized at 780−760°C, entrapped melt portions that contained about 7 wt % H_2O. As the melt content decreased to 5%, its H_2O concentration increased to 11 wt %, the maximum possible value at these $P-T$ parameters. Trend B in Fig. 7a can be explained by the continuing growth/recrystallization of the quartz when the magma ascended from a deep chamber (at approximately 16−18 km) to shallower depths. This ascent was associated with the segregation of CO_2, brines, and aqueous fluid, which progressively depleted in salts, from the magma. This scenario is also well consistent with the variations in Cl concentration in the melt inclusions (Fig. 8): Cl enriched the melt during its deep-seated crystallization and reached a saturation concentration (0.2 wt %), after which it was segregated from the melt in the form of brine and/or more and more diluted solution.

CONCLUSIONS

New experimental data have been obtained on Cl solubility in haplobasalt melts. It has been demonstrated that an increase in NaCl concentration in the fluid results in a decrease in Cl solubility in the melt. The data obtained on Ca and Na partitioning between melt and fluid make it possible to model the evolution of the Ca/Na ratio in the course of crystallization of basaltic melts. Cl solubility in haplogranite melt decreases with increasing K/Na ratio in the melt and fluid. We have also found out that Cl solubility in model granite under a high pressure (10 kbar) increases with increasing H_2O content up to a maximum at an H_2O mole fraction of about 0.6. Inasmuch as the experiments were conducted in the presence of aqueous chloride fluids whose thermodynamic properties are known, we could calculate the thermodynamic parameters of solute species (NaCl, KCl, and $CaCl_2$) in silicate melts. Calculations for the simplest magma−fluid system $Ab-H_2O-NaCl$ highlight the complex character of the phase relations and, hence, also the evolution of H_2O and NaCl concentrations in aluminosilicate melt. We used published data on the composition of melt inclusions in quartz from granites of the Verkhneurmiiskii massif of the Badzhal volcano-plutonic zone (Bortnikov et al., 2019) to demonstrate the complex evolution of the magmatic−fluid system.

SUPPLEMENTARY INFORMATION

The online version contains supplementary material available at https://doi.org/10.1134/S0869591124010028.

CONFLICT OF INTEREST

The authors of this work declare that they have no conflicts of interest.

OPEN ACCESS

REFERENCES

Andreeva, O.A., Yarmolyuk, V.V., Andreeva, I.A., and Borisovskiy, S.E., Magmatic evolution of Changbaishan Tianchi volcano, China−North Korea: evidence from mineral-hosted melt and fluid inclusions, *Petrology,* 2018, vol. 26, no. 5, pp. 515−545.

Aranovich, L.Ya., *Mineral'nye ravnovesiya mnogokomponentnykh tverdykh rastvorov* (Mineral Equilirbia of Multicomponent Solid Solutions), Moscow: Nauka, 1991.

Aranovich, L.Ya., The role of brines in high-temperature metamorphism and granitization, *Petrology,* 2017, vol. 25, no. 5, pp. 486−497.

Aranovich, L.Y. and Newton, R.C., H_2O activity in concentrated NaCl solutions at high pressures and temperatures measured by the brucite−periclase equilibrium, *Contrib. Mineral. Petrol.,* 1996, vol. 125, pp. 200−212.

Aranovich, L.Y. and Newton, R.C., H_2O activity in concentrated KCl and KCl−NaCl solutions at high temperatures and pressures measured by the brucite−periclase equilibrium, *Contrib. Mineral. Petrol.,* 1997, vol. 127, pp. 261−271.

Aranovich, L.Y., Newton, R.C., and Manning, C.E., Brine-assisted anatexis: experimental melting in the system haplogranite−H_2O−NaCl−KCl at deep-crustal conditions, *Earth Planet. Sci. Lett.,* 2013, vol. 374, pp. 111−120.

Aranovich, L.Y. and Safonov, O.G., Halogens in high-grade metamorphism, *The Role of Halogens in Terrestrial and Extraterrestrial Geochemical Processes,* Springer, 2018, pp. 713−757.
https://doi.org/10.1007/978-3-319-61667-4_11

Blundy, J., Afanasyev, A., Tattitch, B., et al., The economic potential of metalliferous sub-volcanic brines, *R. Soc. Open Sci.,* 2021, vol. 8, no. 6.
https://doi.org/10.1098/rsos.202192

Borisov, A. and Aranovich, L.Y., Zircon solubility in silicate melts: new experiments and probability of zircon crystallization in deeply evolved basic melts, *Chem. Geol.,* 2019, vol. 510, pp. 103−112.

Bortnikov, N.S., Aranovich, L.Ya., Kryazhev, S.G., et al., Badzhal tin magmatic−fluid system, Far East, Russia: transition from granite crystallization to hydrothermal ore deposition, *Geol. Ore Deposits,* 2019, vol. 61, no. 3, pp. 199−224.

Chevychelov, V.Y. and Suk, N.I., Influence of the composition of magmatic melt on the solubility of metal chlorides at pressures of 0.1−3.0 kbar, *Petrology,* 2003, vol. 11, pp. 62−74.

Chevychelov, V.Yu., Partitioning of volatile components (Cl, F, and CO_2) in water-saturated fluid−magma systems of various composition, *Petrology,* 2019, vol. 27, no. 6, pp. 585−605.
https://doi.org/10.31857/S0869-5903276638-657

Connolly, J.A.D., Computation of phase equilibria by linear programming: a tool for geodynamic modeling and its application to subduction zone decarbonation, *Earth Planet. Sci. Lett.,* 2005, vol. 236, pp. 524−541.

Connolly, J.A.D., A primer in Gibbs energy minimization for geophysicists, *Petrology,* 2017, vol. 25, pp. 526−534.

Dalou, C. and Mysen, B.O., The effect of H_2O on F and Cl solubility and solution mechanisms of in aluminosilicate melts at high pressure and high temperature, *Am. Mineral.,* 2015, vol. 100, pp. 633−643.

Darken, L.S., Thermodynamics of binary metallic solutions, *Metallurg. Soc. AIME Trans.,* 1967, vol. 239, pp. 80−89.

Dolejš, D. and Zajacz, Z.D.E., Halogens in silicic magmas and their hydrothermal systems, *The Role of Halogens in Terrestrial and Extraterrestrial Geochemical Processes,* Springer, 2018, pp. 431−541.
https://doi.org/10.1007/978-3-319-61667-4_7

Evans, K.A., Mavrogenes, J.A., O'Neill, H.S., et al., A preliminary investigation of chlorine XANES in silicate glasses, *Geochem., Geophys., Geosyst.,* 2008, vol. 9, no. 10.
https://doi.org/10.1029/2008GC002157

Filiberto, J. and Treiman, A.H., The effect of chlorine on the liquidus of basalt: first results and implications for basalt genesis on mars and earth, *Chem. Geol.,* 2009, vol. 263, pp. 60−68.
https://doi.org/10.1016/j.chemgeo.2008.08.025

Goldfarb, R.J. and Pitcairn, I., Orogenic gold: is a genetic association with magmatism realistic?, *Mineral. Deposita,* 2022, vol. 58, pp. 5−35.
https://doi.org/10.1007/s00126-022-01146-8

Holland, H.D., Granites, solutions, and base metal deposits, *Econ. Geol.,* 1972, vol. 67, pp. 281−301.

Holland, T.J.B. and Powell, R., An improved and extended internally consistent thermodynamic dataset for phases of petrological interest, involving a new equation of state for solids, *J. Metamorph. Geol.,* 2011, vol. 29, pp. 333−383.

Hsu, Y-J., Zajacz, Z., Ulmer, P., and Heinrich, C.A., Chlorine partitioning between granitic melt and H_2O−CO_2−NaCl fluids in the earth's upper crust and implications for magmatic-hydrothermal ore genesis, *Geochim. Cosmochim. Acta,* 2019, vol. 261, pp. 171−190.

Ivanov, M.V., Thermodynamic model of the fluid system H_2O−CO_2−NaCl−$CaCl_2$ at *P-T* parameters of the middle and lower crust, *Petrology,* 2023, vol. 31, no. 4, pp. 413−423.

Ivanov M.V., Bushmin S.A., Aranovich L.Ya. Equations of state for NaCl and CaCl2 solutions of arbitrary concentrations at temperatures 423.15−623.15 K and pressures up to 5 kbar, *Dokl. Earth Sci.,* 2018, vol. 481, 1086−1090.

Kouzmanov, K. and Pokrovsky, G.S., Hydrothermal controls on metal distribution in porphyry Cu(−Mo−Au) systems, *Econ. Geol. Spec. Publ.,* 2012, vol. 16, pp. 573−618.

Kovalenko, V.I., Naumov, V.B., Yarmolyuk, V.V., and Dorofeeva, V.A., Volatile components (H_2O, CO_2, Cl, F, and S) in magmas of intermediate and acid compositions from distinct geodynamic settings: evidence from melt inclusions and chill glasses, *Petrology,* 2000, vol. 8, pp. 525−556.

Kusebauch, C., Timm, J., Whitehouse, M.J., et al., Distribution of halogens between fluid and apatite during fluid-mediated replacement processes, *Geochim. Cosmochim. Acta,* 2015, vol. 170, pp. 225−246.

Lukanin O.A. Chlorine partitioning between melt and aqueous chloride fluid during granite magma. Degassing I. Decompression-induced melt degassing, *Geochem. Int.,* 2015, no. 8, pp. 786−810.

Lukanin, O.A., Chlorine partitioning between melt and aqueous chloride fluid phase during granite magma degassing. Part II. Crystallization-induced degassing of melts, *Geochem. Int.,* 2016, vol. 54, no. 8, pp. 660−680.

Papale, P., Moretti, R., and Barbato, D., The compositional dependence of the saturation surface of $H_2O + CO_2$ fluids in silicate melts, *Chem. Geol.,* 2006, vol. 229, pp. 78−95.

Patiño Douce, A.E., Roden, M.F., Chaumba, J., et al., Compositional and the halogen and water budgets of planetary mantles, *Chem. Geol.,* 2011, vol. 288, pp. 14−31.

Rubtsova, E.A., Tagirov B.R., Akinfiev N.N., et al., Coupled solubility of Cu and Ag in chloride-bearing hydrothermal fluids (350−650°C, 1000−1500 bar), *Geol. Ore Deposits,* 2023, vol. 65, no. 1, pp. 11−27.

Ryabchikov, I.D., *Termodinamika flyuidnoi fazy granitoidnykh magm* (Thermodynamics of Fluid Phase of the Granitoid Magmas), Moscow: Nauka, 1975.

Safonov, O.G. and Aranovich, L.Y., Alkali control of high-grade metamorphism and granitization, *Geosci. Front.,* 2014, vol. 5, pp. 711−727.
https://doi.org/10.1016/j.gsf.2014.03.010

Shaposhnikov, V. V. and Aranovich, L.Ya., Experimental study of model granite melting in the presence of alkali carbonate solutions at 400 MPa, *Geochem. Int.,* 2015, vol. 53, no. 9, pp. 838−844.

Shmulovich, K.I. and Graham, C., Plagioclase−aqueous solution equilibrium: concentration dependence, *Petrology,* 2008, vol. 16, pp. 177−192.

Tattitch, B.C. and Blundy, J.D., Cu−Mo partitioning between felsic melts and saline−aqueous fluids as a function of XNaCleq, fo$_2$, and fs$_2$, *Am. Mineral.,* 2017, vol. 102, pp. 1987−2006.
https://doi.org/10.2138/am-2017-5998

Tenner, T.J., Lange, R.A., and Downs, R.T., The albite fusion curve re-examined: new experiments and the high-pressure density and compressibility of high albite and $NaAlSi_3O_8$ liquid, *Am. Mineral.,* 2007, vol. 92, pp. 1573−1585.

Thomas, R.W. and Wood, B.J., The effect of composition on chlorine solubility and behavior in silicate melts, *Am. Mineral.,* 2023, vol. 108, pp. 814−825.

Webster, J.D., Vetere, F., Botcharnikov, R.E., et al., Experimental and modeled chlorine solubilities in aluminosilicate melts at 1 to 7000 bars and 700 to 1250°c: applications to magmas of Augustine Volcano, Alaska, *Am. Mineral.,* 2015, vol. 100, pp. 522−535.

White, R.W., Powell, R., Holland, T.J.B., et al., New mineral activity−composition relations for thermodynamic calculations in metapelitic systems, *J. Metamorph. Geol.,* 2014, vol. 32, pp. 261−286.
https://doi.org/10.1111/jmg.12071

Witham, C.S., Webster, H.N., Hort, M.C., et al., Modeling concentrations of volcanic ash encountered by aircraft in past eruptions, *Atmos. Environ.,* 2012, vol. 48, pp. 219−229.

Translated by E. Kurdyukov